INTERNATIONAL JOURNAL OF
NUMERICAL ANALYSIS AND MODELING
Volume 10, Number 2, Pages 314–332

SEMI-ANALYTICAL NUMERICAL METHODS FOR CONVECTION-DOMINATED PROBLEMS WITH TURNING POINTS

CHANG-YEOL JUNG AND THIEN BINH NGUYEN

(Communicated by Roger Temam)

Abstract. In this article we aim to study finite volume approximations which approximate the solutions of convection-dominated problems possessing the so-called interior transition layers. The stiffness of such problems is due to a small parameter multiplied to the highest order derivative which introduces various transition layers at the boundaries and at the interior points where certain compatibility conditions do not meet. Here, we are interested in resolving interior transition layers at turning points. The proposed semi-analytic method features interior layer correctors which are obtained from singular perturbation analysis near the turning points. We demonstrate this method is efficient, stable and it shows 2^{nd}-order convergence in the approximations.

Key words. Convection-diffusion equations, Singular perturbation analysis, Transition layers, Boundary layers, Compatibility conditions, Turning points, Finite volume methods.

1. Introduction

In this article, we consider a singularly perturbed problem presenting a turning point, that is

$$\begin{cases} L_\epsilon u := -\epsilon u_{xx} - b u_x = f & \text{in } \Omega = (-1,1), \\ u(-1) = u(1) = 0, \end{cases} \tag{1.1}$$

where $0 < \epsilon << 1$, $b = b(x)$, $f = f(x)$ are smooth on $[-1,1]$, and for $\delta > 0$, $b < 0$, for $-\delta < x < 0$, $b(0) = 0$, $b > 0$ for $0 < x < \delta$, and $b_x(0) > 0$.

In our previous work [16], a new numerical approximation to solve a boundary layer problem, i.e., Eq. (1.1) with the sign of $b(x)$ unchanged, is developed and implemented based on enriched subspace techniques. In this paper, we continue to investigate a more challenging problem possessing an interior transition layer, which is displayed near $x = 0$ where the convective coefficient $b(x)$ changes sign. The point $x = 0$ is called a turning point. The asymptotic analysis for problem (1.1) is fully detailed in [14] depending on the compatibility between b and f.

Transition layers are very thin regions, i.e., their thickness is in the order of the small parameter ϵ, where values of the derivative (or gradient in higher dimensional problems) are much larger than those in outer regions of the solution. They appear in the solution when there is a small parameter multiplying the highest derivative and the coefficient of the convective term changes its sign at points called turning points. Transition layers match the discrepancies between outer solutions which occur at turning points. Thus, in the limit case, i.e. when $\epsilon = 0$, singularity happens in the solution around these turning points. This type of singularity is called asymptotic singularity (see e.g. [10], [12] and [26]). Transition layers interpret significant physical phenomena, for instance, turbulent boundary layers occurring

Received by the editors January 18, 2011 and, in revised form, January 19, 2012.
2000 *Mathematics Subject Classification.* 34E15, 80M35, 76R50, 35B40, 80M12.
This work was supported by Basic Science Research Program through the National Research Foundation of Korea (NRF) funded by the Ministry of Education, Science and Technology (2012001167).

at the points where the turbulent boundary layer separates since the tangential velocity vanishes and changes sign at such points (see [3]) in fluid dynamics; or the propagation of light in a nonhomogeneous medium as an application of Maxwell's equations in Electromagnetism (see [1]).

It is well-known that constructing numerical methods for a problem of the type (1.1) is difficult and computationally expensive. It is because very fine meshes are required for the transition layer so that sharp changes in the layer can be accurately captured as well as oscillations due to asymptotic singularity must be prevented from occurring. There are many works devoted to studying the problem, both analytically (see e.g., [8], [9], [14], [17], [23]) and numerically (see e.g., [13], [16], [4], [5], [18]).

Our aim in this article is to construct an accurate and efficient numerical approximation for the solution of Eq. (1.1) based on the technique developed in [16] and the novel asymptotic analysis as in [14]. The advantage of our scheme is that the solution of the transition layer is resolved analytically, thus the mesh size does not rely on the thickness of the layer, leading to a much reduction in computational cost but still preserving the properties of a good approximation mentioned above. The extension to more complex problems, e.g., multiple transition layers, transition layers incorporating boundary layers, or the coefficient $b(x)$ having zeros with multiplicity, etc. is discussed in the Conclusion and will appear in subsequent papers.

The article is organized as follows. In section 2.1, we introduce a conventional finite volume scheme for problem (1.1) (see e.g., [25]). We then employ singular perturbation analysis (see e.g., [9], [14], [19], [20], [22]) in order to derive the exact solution for the transition layer of problem (1.1) in section 2.2. Based on this, a new Finite Volume discretization is introduced in section 2.3. Numerical results illustrating for the methods are presented in section 3. Finally, we close the article with the Conclusion section.

2. Discretizations

To approximate the solution of Eq. (1.1), we employ Finite Volume discretizations. We first introduce a classical finite volume method and then, via singular perturbation analysis, we derive some transition layer correctors which capture the transition layer and spikes caused by the noncompatibility in the data of Eq. (1.1) (see section 2.3.2 below). These correctors are incorporated in the classical scheme to produce a stable, accurate and efficient scheme.

2.1. Classical Finite Volume Method (cFVM). In this section, we apply finite volume discretizations in approximating the solution of Eq. (1.1). Firstly, we define the mesh parameters for our scheme. We rather use a uniform mesh for our computation. Let x_j, u_j be nodal points and values, respectively. The x_j are located at $x = -1 + (j - 1/2)h,\ h = 2/N,\ j = 0, 1, 2, \ldots, N, N + 1$ where h is the mesh size and N is the number of control volumes. The points $x_0,\ x_{N+1}$ are called ghost points or fictitious points which do not belong to the computational domain Ω and their nodal values $u_0,\ u_{N+1}$ are determined via boundary conditions and appropriate interpolations at the boundaries (see (2.6) and (2.7) below). Then the control volumes at x_j have faces at $x_{j-\frac{1}{2}} = x_j - h/2,\ x_{j+\frac{1}{2}} = x_j + h/2,\ j = 1, 2, \ldots, N$. Note that the boundary points are $x_{\frac{1}{2}} = -1,\ x_{N+\frac{1}{2}} = 1$.

For finite volume methods, we use step functions for discretization purposes. Hence, the solution u and its derivative u_x are interpolated as follows:

$$\begin{aligned} u \approx u_h &= \sum_{j=1}^{N} u_j \chi_{(x_{j-\frac{1}{2}},\ x_{j+\frac{1}{2}})}(x), \\ u_x \approx \nabla_h u_h &= \sum_{j=0}^{N} \frac{u_{j+1}-u_j}{h} \chi_{(x_j,\ x_{j+1})}(x), \end{aligned} \tag{2.1}$$

where $u_j = u(x_j)$ and $\chi_{(a,b)}(x)$ is the characteristic function of the interval (a, b).

In [16], it is proved that

$$\begin{cases} |u-u_h|_{L^2(x_{\frac{1}{2}},\ x_{N+\frac{1}{2}})} \le \kappa h |u|_{H^1(x_{\frac{1}{2}},\ x_{N+\frac{1}{2}})}, \\ |u_x - \nabla_h u_h|_{L^2(x_0,\ x_{N+1})} \le \kappa h |u|_{H^2(x_0,\ x_{N+1})}. \end{cases} \tag{2.2}$$

Hence, we are motivated to discretize Eq. (1.1) via (2.1) with the unknown nodal values u_j. The function u_h thus belongs to the finite dimensional space V_h, which is a classical finite volume space, where

$$V_h = \bigoplus_{j=1}^{N} \mathbb{R}\phi_j(.), \tag{2.3}$$

with

$$\phi_j = \phi_j(x) = \chi_{(x_{j-\frac{1}{2}},\ x_{j+\frac{1}{2}})}(x),\ j = 1, \dots, N. \tag{2.4}$$

When we integrate the first derivative over a control volume, i.e.,

$$\int_{x_{j-\frac{1}{2}}}^{x_{j+\frac{1}{2}}} u_x\ dx = u(x_{j+\frac{1}{2}}) - u(x_{j-\frac{1}{2}}), \tag{2.5}$$

we need to interpolate these values using the nodal values u_j, $j = 1, \dots, N$ since u_h is not defined at the volume faces $x_{j-\frac{1}{2}},\ x_{j+\frac{1}{2}}$. Here, we adopt a central difference scheme at faces, including the boundaries:

$$u(-1) = u(x_{\frac{1}{2}}) \approx u_h(x_{\frac{1}{2}}) = \frac{u_0+u_1}{2} = 0, \tag{2.6}$$

$$u(1) = u(x_{N+\frac{1}{2}}) \approx u_h(x_{N+\frac{1}{2}}) = \frac{u_N+u_{N+1}}{2} = 0, \tag{2.7}$$

$$u(x_{j+\frac{1}{2}}) \approx u_h(x_{j+\frac{1}{2}}) = \frac{u_j+u_{j+1}}{2},\ j = 1, \dots, N-1. \tag{2.8}$$

Hence, from (2.1), $\nabla_h u_h$ is,

$$\begin{aligned} \nabla_h u_h = &\frac{2u_1}{h} \chi_{[x_{\frac{1}{2}},\ x_1)}(x) + \frac{-2u_N}{h} \chi_{(x_N,\ x_{N+\frac{1}{2}}]}(x) \\ &+ \sum_{j=1}^{N-1} \frac{u_{j+1}-u_j}{h} \chi_{(x_j,\ x_{j+1})}(x). \end{aligned} \tag{2.9}$$

Eq. (1.1) is discretized by multiplying by the step functions $\chi_{(x_{j-\frac{1}{2}},\ x_{j+\frac{1}{2}})}(x)$ and integrating over Ω, we obtain that

$$-\epsilon u_x \Big|_{x_{j-\frac{1}{2}}}^{x_{j+\frac{1}{2}}} - \int_{x_{j-\frac{1}{2}}}^{x_{j+\frac{1}{2}}} b(x) u_x dx = \int_{x_{j-\frac{1}{2}}}^{x_{j+\frac{1}{2}}} f(x) dx,\ j = 1, \dots, N, \tag{2.10}$$

which is equivalent to

$$(2.11)\quad (-\epsilon u_x - b(x)u)\Big|_{x_{j-\frac{1}{2}}}^{x_{j+\frac{1}{2}}} + \int_{x_{j-\frac{1}{2}}}^{x_{j+\frac{1}{2}}} b_x(x)u\ dx = \int_{x_{j-\frac{1}{2}}}^{x_{j+\frac{1}{2}}} f(x)dx,\ j = 1, \ldots, N.$$

Substituting the approximations (2.1) into Eq. (2.11), we obtain that

$$(2.12)\qquad (-\epsilon \nabla_h u_h - b(x)u_h + b(x)u_j)\Big|_{x_{j-\frac{1}{2}}}^{x_{j+\frac{1}{2}}} = \int_{x_{j-\frac{1}{2}}}^{x_{j+\frac{1}{2}}} f(x)dx,\ j = 1, \ldots, N.$$

Applying the boundary conditions (2.6), (2.7) and arranging terms, we can write the classical finite volume discretization (2.12) as follows, for $j = 1, \ldots, N$,

$$(2.13)\qquad a_{j,j-1}u_{j-1} + a_{j,j}u_j + a_{j,j+1}u_{j+1} = f_j.$$

This system corresponds to (2.41)–(2.42) below with deleting the first row and column.

However, as indicated in the interpolation errors (2.2), if $|u|_{H^1}$, $|u|_{H^2}$ are large, e.g., due to the large gradient of u, the numerical approximation will be poor. Indeed, the classical numerical method experiences severe oscillations (see some numerical examples in section 3 below) near the large gradient of the solution due to the sharp transition layer. To overcome such numerical difficulties, near the sharp layer, we correct the numerical approximation by incorporating appropriate analytic functions which are derived in the following section.

2.2. Singular Perturbation Analysis. Before we proceed, the following example illustrates the sharp variation near the turning point $x = 0$ which is in general difficult to approximate with the classical scheme presented above.

Example 2.1. Consider a two-point boundary problem:

$$(2.14)\qquad \begin{cases} -\epsilon u_{xx} - xu_x = 0 \text{ in } (-1, 1), \\ u(-1) = +1,\ u(1) = -1. \end{cases}$$

Notice that Eq. (2.14) can be rewritten in the form of Eq. (1.1) after changing variables (see, e.g., [14]).

We know that the solution of (2.14) is $u \approx erf\left(-\frac{x}{\sqrt{2\varepsilon}}\right)$, where

$$(2.15)\qquad erf(z) = \frac{2}{\sqrt{\pi}} \int_0^z e^{-s^2} ds.$$

In this example, the characteristics are $x'(t) = -b(x(t)) = -x$ and hence $x' > 0$ for $x \in (-1, 0)$, $x' < 0$ for $x \in (0, 1)$. We thus observe that the characteristics converge to the point $x = 0$. Hence, there is a discontinuity of the outer solutions at the point $x = 0$. In this example, the outer solutions are simply constants. Thus a transition layer is needed to resolve the singularity at $x = 0$ (see Fig. 1). Moreover, a transition layer may also appear due to logarithmic singularity if the forcing term 0 is replaced by $f(x)$ with $f(0) \neq 0$. This is because of the noncompatibility in the data between $b(x)$ and $f(x)$ of the equation. For example, in Eq. (2.14), if $f(x) = 1$, the limit problem (when $\epsilon = 0$) reads $-xu_x = 1$, and thus $u = -ln|x|$ for $|x| > 0$. Here we observe logarithmic singularity at $x = 0$. This issue will be discussed in section 2.3.2.

To understand the local behaviors near a transition layer, we employ techniques of singularly perturbation analysis. Behaviors away from the transition layer are

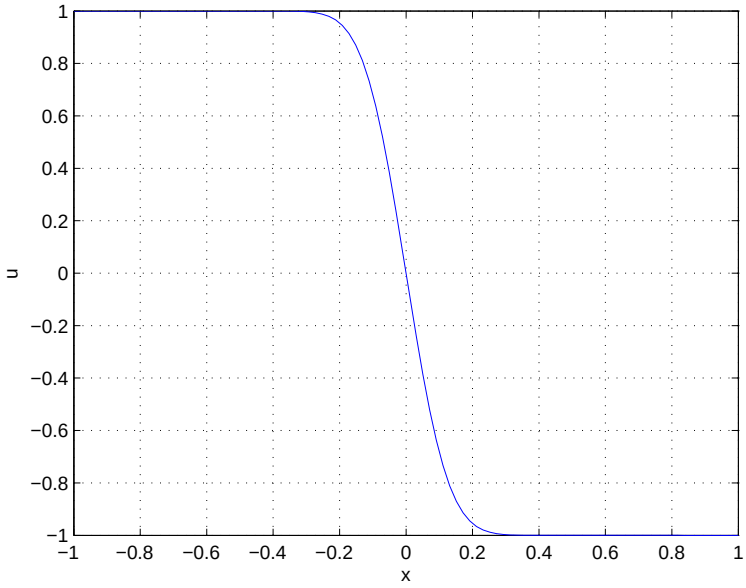

FIGURE 1. Solution of Eq. (2.14) with $\epsilon = 10^{-2}$. The stiff part about $x = 0$ is the transition layer of thickness $\mathcal{O}(\sqrt{\epsilon})$.

determined by the so-called outer expansions or outer solutions which generally display slow variations if f does and is compatible with other data.

Hence, we investigate near the transition layer which arises at a turning point $x = x_0$. For our problem (1.1), the turning point is $x_0 = 0$. We first start with a compatible f, i.e., $f(x_0) = 0 = b(x_0)$. In this case, the outer expansions are considered slow. Using a formal asymptotic expansion for the solution u at the transition layer, and Taylor expansions for b and f about $x = x_0$, we write:

$$u \sim \sum_{k=0}^{\infty} \epsilon^k \theta^k(\bar{x}), \qquad \bar{x} = \frac{x - x_0}{\sqrt{\epsilon}}. \tag{2.16}$$

and

$$b \sim \sum_{k=0}^{\infty} \frac{1}{k!} b_k \bar{x}^k (\sqrt{\epsilon})^k, \qquad f \sim \sum_{k=0}^{\infty} \frac{1}{k!} f_k \bar{x}^k (\sqrt{\epsilon})^k, \tag{2.17}$$

where b_k and f_k are k^{th} order derivatives of b and f with respect to x, respectively, at $x = x_0$. Substituting these expansions into Eq. (1.1) with a note that $b(0) = f(0) = 0$, and balancing terms, we can obtain a system of equations at each order of ϵ. It turns out that, for numerical purposes, the leading term θ^0 suffices to catch the sharp transition layer, which is the solution of

$$-\theta^0_{\bar{x}\bar{x}} - b_1 \bar{x} \theta^0_{\bar{x}} = 0; \tag{2.18}$$

this equation is the zeroth order approximation near $x = 0$ of

$$-\epsilon \theta_{xx} - b(x)\theta_x = 0. \tag{2.19}$$

Transforming Eq. (2.18) back to variable x, we obtain

$$-\epsilon \theta^0_{xx} - b_1 x \theta^0_x = 0; \tag{2.20}$$

whose an explicit form of θ^0 is available:

$$\theta^0 = \frac{2}{\sqrt{\pi}} \int_0^{x\sqrt{\frac{b_1}{2\epsilon}}} e^{-s^2} ds = erf\left(x\sqrt{\frac{b_1}{2\epsilon}}\right). \tag{2.21}$$

The corrector θ^0 will be incorporated into the classical finite volume space V_h to absorb transition layer singularity (see section 2.3). We can infer from the local asymptotic behavior (2.21) that exponentially refined meshes are required at $x = 0$ for the classical numerical method. This leads to expensive computations, even more expensive in higher dimensional problems.

In the case of a noncompatibe f, i.e., $f(0) \neq 0 = b(0)$, as well as the inner expansion, the outer expansions also display sharp transitions like spikes, e.g., logarithm, due to the small variable $b(x)$ and non-degenerate $f(x)$ near $x = 0$. For a detailed analysis, see [14].

In order to resolve the sharp transition due to the noncompatibility between $b(x)$ and $f(x)$ at $x = 0$, we introduce the zeroth corrector φ^0:

$$\varphi^0 = -\int_0^{\frac{x}{\sqrt{\epsilon}}} \int_0^t \exp\left(-b_1 \frac{t^2 - s^2}{2}\right) ds dt. \tag{2.22}$$

The φ^0 is the solution of the equation:

$$-\epsilon \varphi^0_{xx} - b_1 x \varphi^0_x = 1, \tag{2.23}$$

which is the zeroth order approximation near $x = 0$ of

$$-\epsilon \varphi_{xx} - b(x)\varphi_x = 1. \tag{2.24}$$

Using polar coordinates $s = r\cos\theta$, $t = r\sin\theta$ in (2.22), we rewrite $\varphi^0(x)$:

$$\varphi^0(x) = -\frac{1}{b_1} \int_{\frac{\pi}{4}}^{\frac{\pi}{2}} \frac{1}{\cos 2\theta} \left[\exp\left(\frac{b_1 \cos 2\theta}{2\sin^2\theta} \frac{x^2}{\epsilon}\right) - 1\right] d\theta. \tag{2.25}$$

Notice that the double integration (2.22) is transformed to the single one (2.25). Hence, computational cost in the numerical simulations will be much reduced.

From the asymptotic analysis as in [14], in case of a compatible f, we notice that the solution u of Eq. (1.1) can be decomposed into a stiff part (the transition layer), where large values of the derivative are observed, and non-stiff parts (outer expansions) away from the turning point.

We, therefore, introduce a decomposition of the solution u as follows:

$$u = u_s + \lambda\theta^0, \tag{2.26}$$

where u_s is considered a slow variable, θ^0 is the transition layer as in (2.21), and λ is an unknown.

Substituting (2.26) into Eq. (1.1) and using (2.19), we can write:

$$L_\epsilon(u_s + \lambda(\theta^0 - \theta)) = f(x), \text{ in } \Omega, \tag{2.27}$$

which is supplemented with boundary conditions:

$$\begin{cases} u_s(-1) + \lambda\theta^0(-1) = u(-1) = 0, \\ u_s(1) + \lambda\theta^0(1) = u(1) = 0. \end{cases} \tag{2.28}$$

The slow variable u_s will be approximated by the usual step functions and we now propose a new finite volume method in the following section.

2.3. New Finite Volume Method (nFVM). In this section, we present a new approximation method based on Finite Volume to numerically approximate the non-stiff part with the transition layer correctors derived in the previous section. We consider two cases: a single interior transition layer with compatible and non-compatible data.

2.3.1. Compatible Case. Using step functions, we discretize the non-stiff smooth part u_s with finite volumes. From the decomposition (2.26) we approximate u by a new trial function $\tilde{u}_h$,

$$\begin{cases} \tilde{u}_h = u_h + \lambda\theta^0, \\ u_h = \displaystyle\sum_{j=1}^{N} u_j \chi_{(x_{j-\frac{1}{2}},\ x_{j+\frac{1}{2}})}(x). \end{cases} \tag{2.29}$$

Notice that $\tilde{u}_h \approx u$ and $u_h \approx u_s$. As in (2.28), boundary conditions for u_h are as follows:

$$\begin{cases} \tilde{u}_h(x_{\frac{1}{2}}) = u_h(x_{\frac{1}{2}}) + \lambda\theta^0(-1) = 0, \\ \tilde{u}_h(x_{N+\frac{1}{2}}) = u_h(x_{N+\frac{1}{2}}) + \lambda\theta^0(1) = 0, \end{cases} \tag{2.30}$$

where $x_{\frac{1}{2}} = -1,\ x_{N+\frac{1}{2}} = 1$.

Here the mesh data are adopted from the classical Finite Volume in section 2.1.

The function $\tilde{u}_h \approx u$ thus belongs to the finite dimensional space

$$\tilde{V}_h = V_h \oplus \mathbb{R}\theta^0(.), \tag{2.31}$$

where V_h is defined in (2.3).

We now discretize Eq. (2.27) with (2.28). Since θ^0 is asymptotically close to θ, the term $\theta^0 - \theta$ is small and absorbed in other entries in the discrete system (2.41)–(2.42). Hence, we may drop $\lambda(\theta^0 - \theta)$. If necessary, to achieve higher accuracy, we can introduce a higher asymptotic expansion which replaces θ^0. Since u_s is slow, as we did in the classical scheme, using a central difference method at faces including the boundaries, from (2.30) we write that

$$u_s(-1) = u_s(x_{\frac{1}{2}}) \approx u_h(x_{\frac{1}{2}}) = \frac{u_0 + u_1}{2} = -\lambda\theta^0(-1), \tag{2.32}$$

$$u_s(1) = u_s(x_{N+\frac{1}{2}}) \approx u_h(x_{N+\frac{1}{2}}) = \frac{u_N + u_{N+1}}{2} = -\lambda\theta^0(1), \tag{2.33}$$

$$u_s(x_{j+\frac{1}{2}}) \approx u_h(x_{j+\frac{1}{2}}) = \frac{u_j + u_{j+1}}{2},\ j = 1, \ldots, N-1. \tag{2.34}$$

In the same way, we write a new approximation for u_x as follows, for $h = h_j = x_{j+1} - x_j$,

$$\begin{cases} \nabla_h \tilde{u}_h = \nabla_h u_h + \lambda\theta^0_x, \\ \nabla_h u_h = \displaystyle\sum_{j=0}^{N} \frac{u_{j+1} - u_j}{h} \chi_{(x_j,\ x_{j+1})}(x). \end{cases} \tag{2.35}$$

Notice that $\nabla_h \tilde{u}_h \sim u_x$ and $\nabla_h u_h \sim u_{sx}$. Using the boundary conditions (2.32) and (2.33), the numerical derivative $\nabla_h u_h$ can be rewritten as:

$$\begin{aligned} \nabla_h u_h = {} & \frac{2u_1 + 2\lambda\theta^0(-1)}{h} \chi_{[x_{\frac{1}{2}},\ x_1)}(x) + \frac{-2\lambda\theta^0(1) - 2u_N}{h} \chi_{(x_N,\ x_{N+\frac{1}{2}}]}(x) \\ & + \sum_{j=1}^{N-1} \frac{u_{j+1} - u_j}{h} \chi_{(x_j,\ x_{j+1})}(x). \end{aligned} \tag{2.36}$$

With respect to the unknown λ, we first multiply (2.27) by the test function θ^0 and integrate over Ω. However, as a test function, θ^0 is expected to make the stiffness matrix highly ill-conditioned because θ^0 is almost constant except at a small neighborhood of the turning point $x = 0$, and the constants are easily approximated by other test functions, i.e., step functions. Hence, we modify θ^0 to be much distinguished from the linear combination of other test step functions and we thus define the test function ϕ which satisfies zero boundary conditions:

$$\phi = \theta^0 - \theta^0(1)x. \tag{2.37}$$

Multiplying (2.27) by ϕ and integrating over the domain Ω, after dropping the term $\lambda(\theta^0 - \theta)$, we obtain that

$$\int_{-1}^{1} u_{sx}(\epsilon\phi_x - b(x)\phi) = \int_{-1}^{1} f(x)\phi, \tag{2.38}$$

and using the approximations (2.35)–(2.36), we find that

$$\begin{aligned} &\frac{2u_1 + 2\lambda\theta^0(-1)}{h} I(-1, -1 + \frac{1}{2}h) + \frac{-2\lambda\theta^0(1) - 2u_N}{h} I(1 - \frac{1}{2}h, 1) \\ &+ \sum_{j=1}^{N-1} \frac{u_{j+1} - u_j}{h} I(x_j,\ x_{j+1}) = \int_{-1}^{1} f(x)\phi, \end{aligned} \tag{2.39}$$

where $I(a, b) = \int_a^b (\epsilon\phi_x - b(x)\phi)$.

We then obtain the equation as follows:

$$a_{00}\lambda + a_{01}u_1 + a_{0N}u_N + \sum_{j=2}^{N-1} a_{0j}u_j = f_0, \tag{2.40}$$

which corresponds to the first row and column of the system (2.41) − (2.42) below.

From Eq. (2.27), dropping the term $\lambda(\theta^0 - \theta)$, we then derive the same discretized equation as (2.12) with u_h, ∇u_h of the conventional scheme replaced by the new approximations $\tilde{u}_h$, $\nabla_h \tilde{u}_h$ as in Eqs. (2.29) and (2.35). Then using the boundary conditions (2.32)–(2.34), we can similarly obtain the same system as Eq. (2.13). Combining with the additional Eq. (2.40), we obtain a discrete system which incorporates the corrector θ^0:

$$\mathcal{A}\mathbf{u} = \mathbf{f}, \tag{2.41}$$

where $\mathcal{A} = \mathcal{A}_\epsilon = (a_{ij}^\epsilon), \mathbf{u} = (\lambda, u_1, \dots, u_N)^T, \mathbf{f} = (f_0, f_1, \dots, f_N)^T$, and for $i, j = 0, \dots, N,\ l = 2, \dots, N-1,\ m = 1, \dots, N$ with

$$
\begin{cases}
a_{00} = \dfrac{2}{h}\Big[\theta^0(-1)I(-1, -1+\frac{1}{2}h) - \theta^0(1)I(1-\frac{1}{2}h, 1)\Big], \\
a_{01} = \dfrac{1}{h}\Big[2I(-1, -1+\frac{1}{2}h) - I(-1+\frac{1}{2}h, -1+\frac{3}{2}h)\Big], \\
a_{0l} = \dfrac{1}{h}\Big[I(-1+(l-\frac{3}{2})h, -1+(l-\frac{1}{2})h) \\
\qquad\qquad -I(-1+(l-\frac{1}{2})h, -1+(l+\frac{1}{2})h)\Big], \\
a_{0N} = \dfrac{1}{h}\Big[-2I(1-\frac{1}{2}h, 1) + I(1-\frac{3}{2}h, 1-\frac{1}{2}h)\Big], \\
a_{10} = \Big[\dfrac{2\epsilon}{h} - b(-1)\Big]\theta^0(-1), \\
a_{11} = \dfrac{3\epsilon}{h} + \dfrac{1}{2}b(x_{\frac{3}{2}}) - b(-1), \\
a_{12} = -\dfrac{\epsilon}{h} - \dfrac{1}{2}b(x_{\frac{3}{2}}), \\
a_{l,l-1} = -\dfrac{\epsilon}{h} + \dfrac{1}{2}b(x_{l-\frac{1}{2}}), \\
a_{l,l} = \dfrac{2\epsilon}{h} + \dfrac{1}{2}\Big[b(x_{l+\frac{1}{2}}) - b(x_{l-\frac{1}{2}})\Big], \\
a_{l,l+1} = -\dfrac{\epsilon}{h} - \dfrac{1}{2}b(x_{l+\frac{1}{2}}), \\
a_{N0} = \Big[\dfrac{2\epsilon}{h} + b(1)\Big]\theta^0(1), \\
a_{N,N-1} = -\dfrac{\epsilon}{h} + \dfrac{1}{2}b(x_{N-\frac{1}{2}}), \\
a_{N,N} = \dfrac{3\epsilon}{h} - \dfrac{1}{2}b(x_{N-\frac{1}{2}}) + b(1), \\
f_0 = \int_{-1}^{1} f(x)\phi, \\
f_m = \int_{x_{m-\frac{1}{2}}}^{x_{m+\frac{1}{2}}} f(x),
\end{cases}
\tag{2.42}
$$

and all other entries vanish. Here, we recall $I(a,b) = \int_a^b (\epsilon\phi_x - b(x)\phi)$. Notice that the system (2.41)–(2.42) is tridiagonal, except for the first row, and can be solved easily by using the sparsity of $\mathcal{A}$.

2.3.2. Noncompatible Case. In this section, we present a numerical approximation scheme for the solution of Eq. (1.1) where $b(x)$ and $f(x)$ are noncompatible, i.e., when $f(0) \neq 0 = b(0)$.

We, therefore, introduce a new decomposition for the approximation of the solution of (1.1) as follows:

$$u = u_s + \lambda\theta^0 + f(0)\varphi^0. \tag{2.43}$$

Substituting (2.43) into Eq. (1.1) and using (2.19), (2.24), we obtain that

$$L_\epsilon(u_s + \lambda(\theta^0 - \theta) + f(0)(\varphi^0 - \varphi)) = f(x) - f(0), \text{ in } \Omega. \tag{2.44}$$

Since θ^0, φ^0 are asymptotically close to θ, φ, respectively, similarly we may drop the terms $\lambda(\theta^0 - \theta)$, $f(0)(\varphi^0 - \varphi)$. Higher order asymptotic terms which replace θ^0, φ^0 can be adapted for higher accurate schemes, if necessary.

TABLE 1. Comparison on L^2 and L^∞ errors of the classical FVM (cFVM) and the new FVM (nFVM) using the corrector θ^0 with the exact solution (3.2) of Eq. (3.1) with different values of ϵ and numbers of control volumes N.

		cFVM		nFVM	
ϵ	N	L^2 error	L^∞ error	L^2 error	L^∞ error
10^{-1}	40	1.200E-03	1.800E-03	9.429E-04	1.700E-03
10^{-1}	80	3.029E-04	4.695E-04	2.362E-04	4.413E-04
10^{-1}	160	7.573E-05	1.189E-04	5.904E-05	1.123E-04
10^{-1}	320	1.893E-05	2.990E-05	1.477E-05	2.828E-05
10^{-2}	40	1.600E-03	2.300E-03	1.800E-03	2.600E-03
10^{-2}	80	3.820E-04	5.617E-04	4.543E-04	6.555E-04
10^{-2}	160	9.476E-05	1.372E-04	1.135E-04	1.633E-04
10^{-2}	320	2.365E-05	3.439E-05	2.838E-05	4.883E-05
10^{-3}	40	1.650E-02	4.240E-02	**2.600E-03**	**6.700E-03**
10^{-3}	80	2.400E-03	8.800E-03	**5.637E-04**	**1.400E-03**
10^{-3}	160	5.560E-04	2.000E-03	**1.392E-04**	**3.310E-04**
10^{-3}	320	1.366E-04	4.982E-04	**4.470E-05**	**8.400E-05**
10^{-4}	40	3.150E-02	8.630E-02	**2.200E-03**	**4.200E-03**
10^{-4}	80	2.390E-02	6.940E-02	**1.100E-03**	**3.400E-03**
10^{-4}	160	4.500E-03	2.280E-02	**1.907E-04**	**8.462E-04**
10^{-4}	320	8.474E-04	5.300E-03	**4.192E-05**	**1.961E-04**
10^{-5}	40	4.900E-03	1.330E-02	**1.800E-03**	**2.400E-03**
10^{-5}	80	1.100E-02	4.240E-02	**4.817E-04**	**9.954E-04**
10^{-5}	160	1.840E-02	9.540E-02	**2.975E-04**	**1.300E-03**
10^{-5}	320	9.200E-03	6.300E-02	**1.063E-04**	**7.367E-04**

TABLE 2. Comparison on L^2 and L^∞ errors of the cFVM and the nFVM with the exact solution (3.2) of Eq. (3.1), $N = 160$.

ϵ	cFVM		nFVM	
	L^2 error	L^∞ error	L^2 error	L^∞ error
10^{-1}	7.573E-05	1.189E-04	5.904E-05	1.123E-04
10^{-2}	9.476E-05	1.372E-04	1.135E-04	1.633E-04
10^{-3}	5.560E-04	2.000E-03	1.392E-04	3.310E-04
10^{-4}	4.500E-03	*2.280E-02*	**1.907E-04**	**8.462E-04**
10^{-5}	1.840E-02	*9.540E-02*	**2.975E-04**	**1.300E-03**
10^{-6}	3.300E-03	*1.750E-02*	**1.158E-04**	**2.332E-04**

The right-hand side $f(x) - f(0)$ is compatible with $b(x)$ at $x = 0$, and the logarithmic singularity is analytically resolved.

Eq. (2.44) is supplemented with boundary conditions:

$$\begin{cases} u_s(-1) + \lambda\theta^0(-1) + f(0)\varphi^0(-1) = u(-1) = 0, \\ u_s(1) + \lambda\theta^0(1) + f(0)\varphi^0(1) = u(1) = 0. \end{cases} \tag{2.45}$$

Applying the new method to (2.44) and dropping the terms $\lambda(\theta^0 - \theta)$, $f(0)(\varphi^0 - \varphi)$, we obtain the system (2.41)–(2.42) with the following modification in $\mathbf{f}$, due to

the boundary conditions (2.45):

$$
\begin{cases}
f_0 = -\dfrac{2}{h}\Big[I(-1,-1+\dfrac{1}{2}h)f(0)\varphi^0(-1) - I(1-\dfrac{1}{2}h,1)f(0)\varphi^0(1)\Big] \\
\qquad\quad + \int_{-1}^{1}(f(x)-f(0))\phi, \\
f_1 = -\Big(\dfrac{2\epsilon}{h} - b(-1)\Big)f(0)\varphi^0(-1) + \int_{x_{\frac{1}{2}}}^{x_{\frac{3}{2}}}(f(x)-f(0)), \\
f_N = -\Big(\dfrac{2\epsilon}{h} + b(1)\Big)f(0)\varphi^0(1) + \int_{x_{N-\frac{1}{2}}}^{x_{N+\frac{1}{2}}}(f(x)-f(0)), \\
f_m = \int_{x_{m-\frac{1}{2}}}^{x_{m+\frac{1}{2}}}(f(x)-f(0)),\ m = 2,\ldots,N-1.
\end{cases}
\tag{2.46}
$$

Remark 2.1. For both compatible and noncompatible cases, we use the same discretizations u_h and $\nabla_h u_h$ to approximate u_s and u_{sx}, respectively. The former is the same for both cases as well as for the classical scheme, but the latter is different due to the boundary conditions as in (2.6), (2.7) for the classical scheme, (2.30) for the compatible case, and (2.45) for the noncompatible case.

3. Numerical Results

In this section, we present a number of examples to illustrate the accuracy and efficiency of our new method.

3.1. Compatible Case. We first consider the compatible case where condition $b(0) = 0 = f(0)$ is satisfied. We rewrite Eq. (1.1) with the right-hand side $f(x)$ specified as below:

$$
\begin{cases}
-\epsilon u_{xx} - x u_x = f(x) = 3erf\left(\dfrac{1}{\sqrt{2\epsilon}}\right)(x^3 + 2\epsilon x), \\
u(-1) = u(1) = 0.
\end{cases}
\tag{3.1}
$$

An exact solution is available for Eq. (3.1), which is as follows:

$$
u_e = erf\left(\frac{x}{\sqrt{2\epsilon}}\right) - erf\left(\frac{1}{\sqrt{2\epsilon}}\right)x^3. \tag{3.2}
$$

We approximate the solution of Eq. (3.1) with the classical and new FVM schemes (cFVM, nFVM). For the nFVM, the corrector $\lambda\theta^0$ with the zeroth term θ^0 as in (2.21) is used in the simulation. We notice that only the non-stiff part u_s as in (2.26) is approximated by solving the system (2.41)–(2.42). The numerical solution $\tilde{u}_h$, is then constructed by using the decomposition (2.29).

Results for both schemes are plotted, together with the exact solution (3.2), in Fig. 2 with $\epsilon = 10^{-4}$ and mesh size $h = 2/N = 2/40$. As indicated in the interpolation errors (2.2), with such a coarse mesh, the cFVM exhibits oscillations near the turning point (see also Figs. 7 and 9); whereas the nFVM well captures the sharp transition layer. We recall that the transition layer of the nFVM is an analytical solution, captured by the corrector $\lambda\theta^0$ where θ^0 is the zeroth term of the asymptotic expansion as in (2.20)–(2.19). Furthermore, meshes used for the transition layer of the new method are *uniform and independent of* the small parameter ϵ. We notice that in case of the cFVM scheme, exponentially refined meshes are required near the transition layer. Hence, the former is *much more efficient than* the latter scheme.

Numerical errors, measured in L^2 and L^∞ norms, of the two schemes are estimated and listed in Table 1, with a variety in values of ϵ and mesh sizes h, and in Table 2, with a fixed mesh size $h = 2/N = 2/160$. It is shown that the nFVM shows

much better accuracy for small values of ϵ and both cFVM and nFVM schemes have the same order of accuracy for $\epsilon \geq 10^{-2}$. Furthermore, as indicated in Table 2, the nFVM is *very robust* with respect to changes in ϵ, whereas the cFVM loses accuracies as ϵ tends to be small.

Since the cFVM cannot capture the singularity of the transition layer, the errors caused by oscillations near them contaminate the accuracy of the whole computational domain Ω. Hence, the nFVM is *more stable* and, in general, *more accurate than* cFVM. This conclusion is depicted in Fig. 3 where numerical errors of both schemes are plotted with $\epsilon = 10^{-4}$ and different mesh sizes h. For Figs. 3 and 4– 5 discussed below, we plot the errors in log scale vs. n where $N = 2^n \times 10$ is the number of control volumes.

In Figs. 4 and 5, L^2 and L^∞ errors of the new scheme are plotted with different values of ϵ and mesh sizes h. From the figures, we draw two conclusions. Firstly, 2^{nd}-order convergence is achieved for the new method. Secondly, there are differences between the errors of the outer and inner solutions, which are most clearly seen in L^∞ errors (see Fig. 5) where the plots depend on ϵ linearly in log scales. This is due to asymptotic errors because in the inner expansion, only the zeroth term θ^0 (see (2.20), (2.19), and (2.21)) is used as the corrector in the decomposition (2.26). The asymptotically small term $\lambda(\theta^0 - \theta)$ in (2.27) is dropped and considered absorbed by other entries in the system (2.41)–(2.42). It can be also seen in Table 1. In case of $\epsilon = 10^{-5}$, there is an increase in the L^∞ errors for the nFVM when the mesh is refined from $N = 160$ to $N = 320$. This discrepancy can be reduced if more asymptotic terms are introduced in the corrector, in case higher order of accuracy is required.

In Fig. 6, different right-hand side functions $f(x)$ are simulated to illustrate the robustness of the new method for the compatible case.

3.2. Non-compatible Case. In this section, examples for the noncompatible case are given. We first consider the following problem:

$$\begin{cases} -\epsilon u_{xx} - x u_x = f(x) = \cos\left(\dfrac{\pi}{2}x\right) + x, \\ u(-1) = u(1) = 0. \end{cases} \tag{3.3}$$

Here, $b(0) = 0$ and $f(0) = 1$. Hence, $b(x)$ and $f(x)$ are noncompatible. We apply the decomposition (2.43) with adding the zeroth corrector φ^0, the boundary conditions as in (2.45). The system (2.41)–(2.42) are then solved with $\mathbf{f}$ modified as in (2.46). Numerical solutions from the cFVM and nFVM are shown in Fig. 7. As in the compatible case, the nFVM scheme well resolves the asymptotic and logarithmic singularity and there are oscillations in case of the cFVM scheme in both outer and inner regions. The oscillations are much stronger than those in the compatible case. However, the nFVM scheme is very robust and captures the large gradient near the transition layer for both compatible and noncompatible cases.

In Fig. 8, more examples are given to illustrate for the noncompatible case with $b(x) = x$ and different $f(x)$'s on the right-hand side of Eq. (3.3). It can be seen that logarithmic singularity is very well resolved.

The last example is tested for the case when $b(x) = \sin x$ with $f(x) = x$ and $f(x) = 1$ for a compatible and noncompatible case, respectively. We notice that the same correctors, θ^0 as in (2.21) and φ^0 as in (2.22), are applied in this simulation because only the zeroth terms, which approximate (2.19) and (2.24), respectively, are used as the correctors. Results are plotted in Fig. 9 for the compatible case, Fig. 10 for the noncompatible case.

4. Conclusion

In this paper, we have proposed a new numerical method based on finite volume approach to approximate stiff problems having an interior transition layer near a turning point $x = x_0$. Firstly, the analytical solution θ for the transition layer is derived by employing singular perturbation analysis. It turned out that only the zeroth term θ^0 is enough for numerical purposes. However, in higher order schemes, more asymptotic terms as in (2.16) will be needed. This layer, incorporating with an unknown λ, is added to enrich the classical finite volume space.

The problem has been also studied in a more complicated case with the occurrence of logarithmic singularity near the turning point due to the noncompatibility in the data of the problem. One more corrector φ as in (2.24) is added into the solution decomposition as in (2.43) so that the problem can be transformed into a compatible case analytically. Hence, the new scheme can now be applied; new boundary conditions (2.45) are then imposed, and thus the right-hand side $\mathbf{f}$ is modified as in (2.46).

A variety of examples are given to illustrate the accuracy, stability and efficiency of the new method in section 3 with different coefficients $b(x)$ and right-hand side functions *f(x)*, both for compatible and noncompatible cases.

The technique presented in this article can be further developed for more complex cases. If we have multiple transition layers at $x = x_j$, introducing a Lagrange interpolating polynomial, we write:

$$P_j(x) = \prod_{\substack{k=1 \\ k\neq j}}^{n} \frac{x - x_k}{x_j - x_k}, \;\; f(x) = \sum_{l=1}^{n} P_l(x) f(x). \tag{4.1}$$

Here, we used the fact that $Q(x) := \sum_{l=1}^{n} P_l(x) = 1$ because $Q(x_j) = 1,\ j = 1, 2, \ldots, n$ and $Q(x)$ is of degree $n - 1$. Then $P_j(x)f(x) = 0$ at $x = x_l,\ l = 1, 2, \ldots, n,\ l \neq j$, but $P_j(x)f(x)$ may not be compatible at $x = x_j$, i.e., $P_j(x_j)f(x_j) = f(x_j) \neq 0$. For this single noncompatible point x_j, we have already treated in the text.

Writing the solution of Eq. (1.1) $u = \sum_{j=1}^{n} v^j$ where

$$L_\epsilon(v^j) = P_j(x)f(x), \;\; v^j = 0 \text{ at } x = \pm 1, \tag{4.2}$$

and applying the numerical techniques in the text to each equation (4.2), thanks to the superposition of the solutions, we finally obtain the numerical solution u_N for u. Parallel computing in this case is well suited because Eq. (4.2) can be solved independently at each processor $j,\ j = 1, 2, \ldots, n$.

Combining with the previous results (see e.g. [16]), boundary layer correctors can be also incorporated, and if the coefficient $b(x)$ has zeros at $x = x_j$ with multiplicity, the form of the correctors should be changed according to the singular perturbation analysis at $x = x_j$. All these changes can be adapted without difficulties. For instance, if $b(x) = (x - 1/2)(x + 1/2)$ in the model (1.1), there are a boundary layer at the outflow $x = -1$ and a transition layer at the turning point $x = 1/2$. Or in multi-dimensional problems, the derivative in the convective term is replaced by the gradient of $u(x)$. For nonlinear problems, their linearized version can be taken into account to find out appropriate correctors. These issues will be discussed in forthcoming papers.

References

[1] I. Andronov, D. Bouche and F. Molinet, *Asymptotic and hybrid methods in electromagnetics,* IEE Electromagnetic Waves Series 48, 2005.

[2] Claude Bardos, *Problèmes aux limites pour les équations aux dérivées partielles du premier ordre à coefficients réels; théorèmes d'approximation; application à l'équation de transport. (French)* Ann. Sci. Ecole Norm. Sup. (4) 3 1970, pp 185-233.

[3] G. K. Batchelor, *An Introduction to Fluid Dynamics*, Cambridge University Press, Cambridge, 1988.

[4] W. Cheng and R. Temam, *Numerical approximation of one-dimensional stationary diffusion equations with boundary layers*, Comput. Fluids **31**, 453-466 (2002)

[5] W. Cheng, R. Temam, and X. Wang, *New approximation algorithms for a class of partial differential equations displaying boundary layer behavior*, Methods Appl. Anal. **7**, 363-390 (2000).

[6] A. J. Desanti, *Nonmonotone interior layer theory for some singularly perturbed quasilinear boundary value problems with turning points*, SIAM J. Math. Anal. **18**, 321-331 (1987).

[7] P. G. Drazin and W. H. Reid, *Hydrodynamic Stability, 2nd ed.*, Cambridge University Press, Cambridge, 2004.

[8] W. Eckhaus, *Boundary layers in linear elliptic singular perturbations*, SIAM Rev. **14**, 225-270 (1972).

[9] W. Eckhaus and E. M. de Jager, *Asymptotic solutions of singular perturbation problems for linear differential equations of elliptic type,* Arch. Rational Mech. Anal. **23**, pp 26-86 (1966).

[10] M. H. Holmes, *Introduction to Perturbation Methods*, Springer, New York, 1995.

[11] H. Han and R. B. Kellogg, *A method of enriched subspaces for the numerical solution of a parabolic singular perturbation problem.* In: Computational and Asymptotic Methods for Boundary and Interior Layers, Dublin, pp.46-52 (1982).

[12] R. S. Johnson, *Singular Perturbation Theory*, Springer Science+Business Media, Inc., New York, 2005.

[13] C. Jung and R. Temam, *Numerical approximation of two-dimensional convection-diffusion equations with multiple boundary layers*, Internat. J. Numer. Anal. Model. **2**, 367.408 (2005).

[14] C. Jung and R. Temam, *Asymptotic analysis for singularly perturbed convection-diffusion equations with a turning point*, J. Mathematical Physics, **48**, 065301 (2007).

[15] C. Jung, *Finite elements scheme in enriched subspaces for singularly perturbed reaction-diffusion problems on a square domain*, Asymptot. Anal. **57**, 41-69 (2008).

[16] C. Jung and R. Temam, *Finite volume approximation of one-dimensional stiff convection-diffusion equations.* J. Sci. Comput. **41**, no. 3, pp 384-410. (2009).

[17] R. B. Kellogg and M. Stynes, *Layers and corner singularities in singularly perturbed elliptic problems*, BIT **48**(2), 309-314 (2008).

[18] I. Kalashnikova, R. Tezaur, C. Farhat, *A Discontinuous Enrichment Method for Variable Coefficient Advection-Diffusion at High Peclet Number*, Int. J. Numer. Meth. Engng. **87**, (2010) 309-335.

[19] J. L. Lions, *Perturbations Singulières dans les Problèmes aux Limites et en Contrôle Optimal (in French)*, Lecture Notes in Mathematics Vol. 323, Springer, Berlin, 1973.

[20] R. E. O'Malley, *Singularly perturbed linear two-point boundary value problems.* SIAM Rev. **50** (2008), no. 3, pp 459-482.

[21] M. Stynes, *Steady-state convection-diffusion problems*, Acta Numer., **14** (2005), 445–508.

[22] S. Shih and R. B. Kellogg, *Asymptotic analysis of a singular perturbation problem.* Siam J. Math. Anal. **18** (1987), pp . 1467-1511.

[23] R. Temam and X. Wang, *Boundary layers associated with incompressible Navier-Stokes equations: the noncharacteristic boundary case.* J. Differ. Equ., **179** (2002), no. 2, 647–686.

[24] M. I. Vishik and L. A. Lyusternik, *Regular degeneration and boundary layer for linear differential equations with small parameter*, Usp. Mat. Nauk **12**, 3.122 (1957).

[25] H.K. Versteeg and W. Malalasekera, *An Introduction to Computational Fluid Dynamics: The Finite Volume Method, 2nd ed.*, Pearson/Prentice Hall, 2007.

[26] W. Wasow, *Linear Turning point Theory*, Spinger, New York, 1985.

Ulsan National Institute of Science and Technology, Banyeon-ri 100, Eonyang-eup, Ulju-gun, Ulsan, Republic of Korea

E-mail: `cjung@unist.ac.kr and thienbinh84@unist.ac.kr`

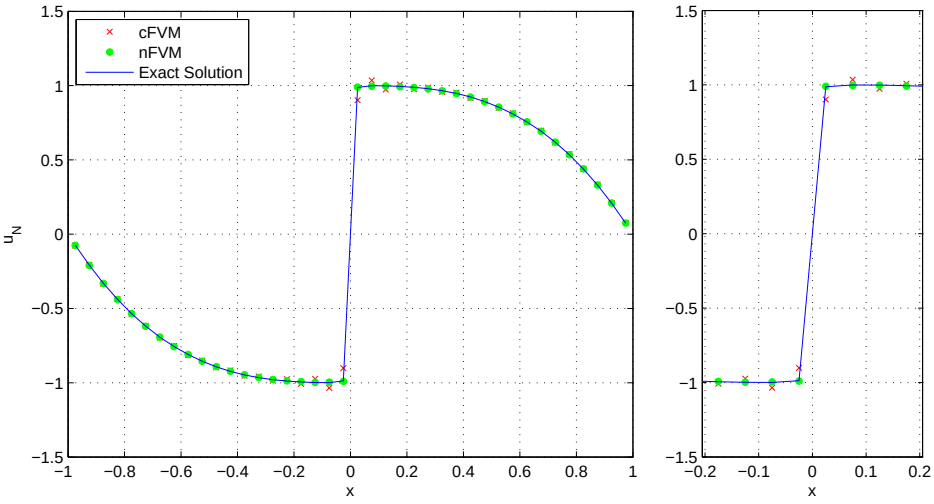

FIGURE 2. **(a)** Numerical solutions u_N of Eq. (3.1) from the classical FVM (cFVM) vs. new FVM (nFVM) using corrector θ^0: $\epsilon = 10^{-4}$, $N = 40$; **(b)** Zooming near the transition layer.

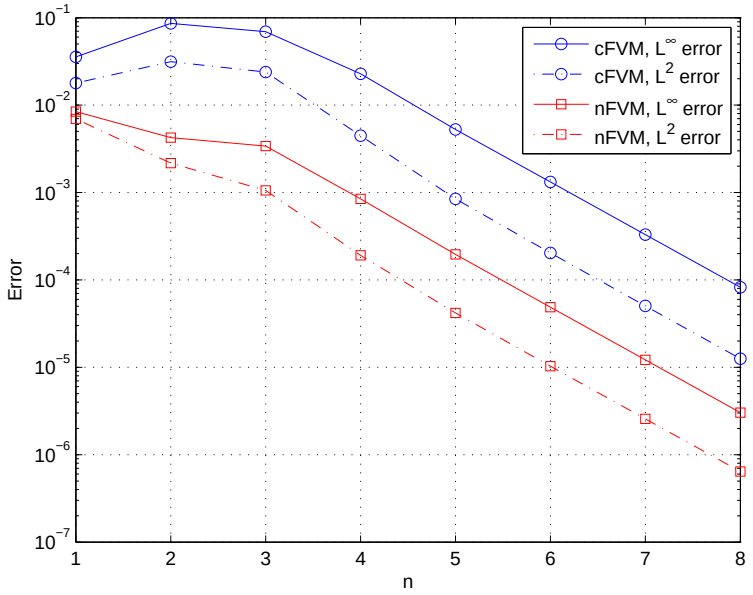

FIGURE 3. Error plotting of numerical solutions of Eq. (3.1) from the cFVM vs. nFVM: $\epsilon = 10^{-4}$, $N = 2^n \times 10$ is the number of control volumes.

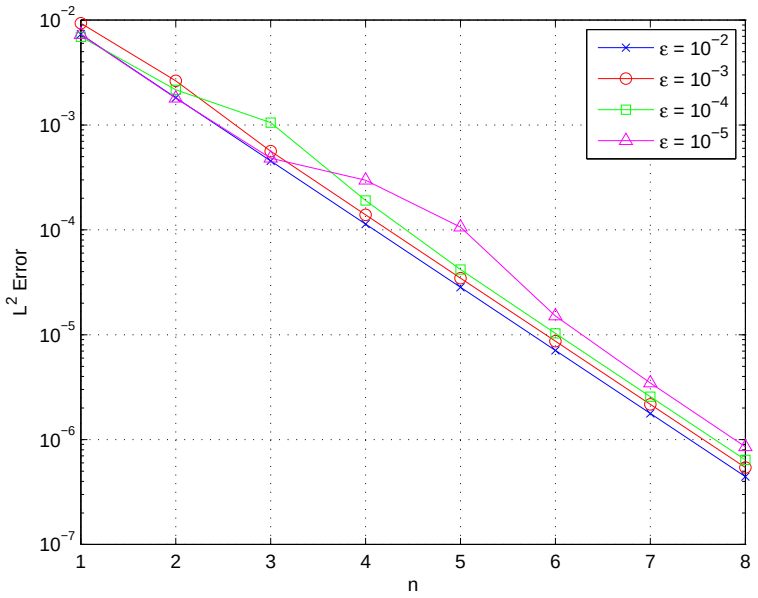

FIGURE 4. L^2 error plotting of numerical solutions of Eq. (3.1) from the nFVM with different values of ϵ, $N = 2^n \times 10$ is the number of control volumes.

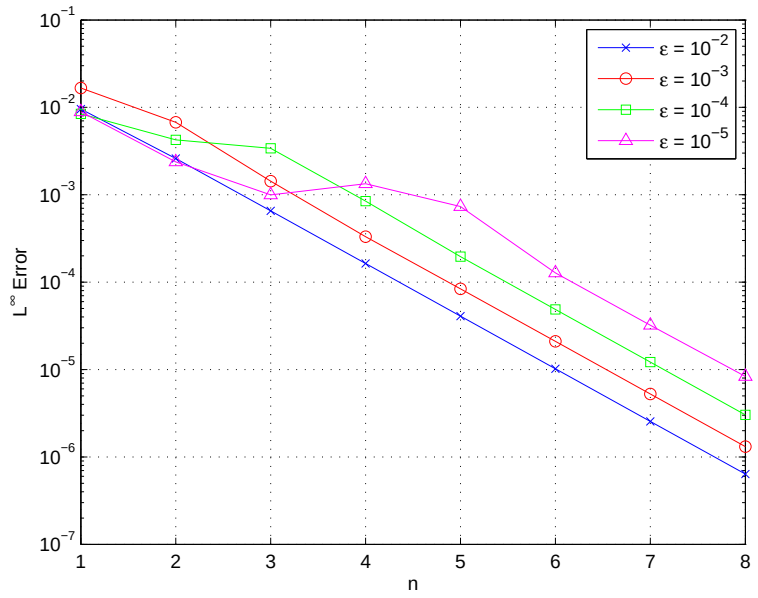

FIGURE 5. L^∞ error plotting of numerical solutions of Eq. (3.1) from the nFVM with different values of ϵ, $N = 2^n \times 10$ is the number of control volumes.

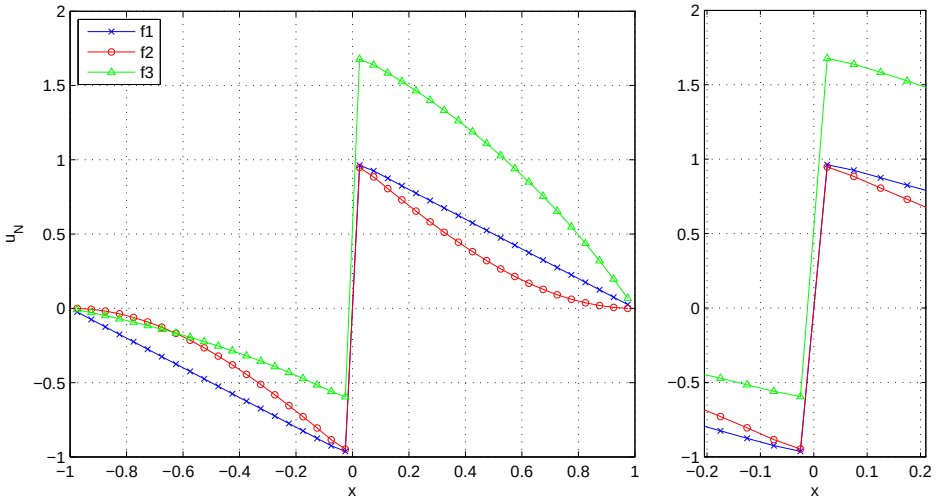

(a) (b)

FIGURE 6. **(a)** Numerical solutions u_N from nFVM with $b(x) = x$ and $f(x) = f_j(x)$ for the compatible case: $f_1(x) = x$, $f_2(x) = -\frac{\pi}{2} erf\left(\frac{1}{\sqrt{2\epsilon}}\right)\left[\frac{\pi}{2}\epsilon \sin\left(\frac{\pi}{2}x\right) - x\cos\left(\frac{\pi}{2}x\right)\right]$, $f_3(x) = xe^x$, $\epsilon = 10^{-4}$, $N = 40$; **(b)** Zooming near the transition layer.

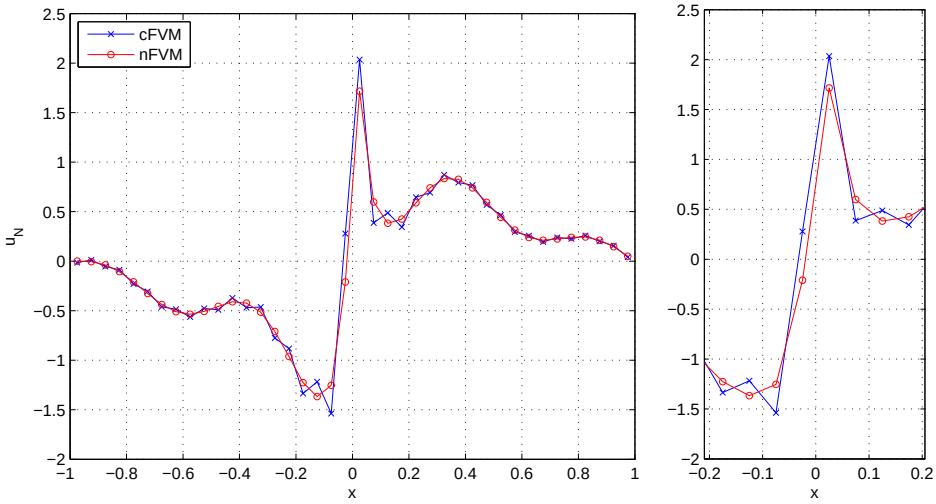

(a) (b)

FIGURE 7. **(a)** Numerical solutions u_N of Eq. (3.3) from the cFVM vs. nFVM using two correctors θ^0 and φ^0: $\epsilon = 10^{-4}$, $N = 40$ for the noncompatible case; **(b)** Zooming near the transition layer.

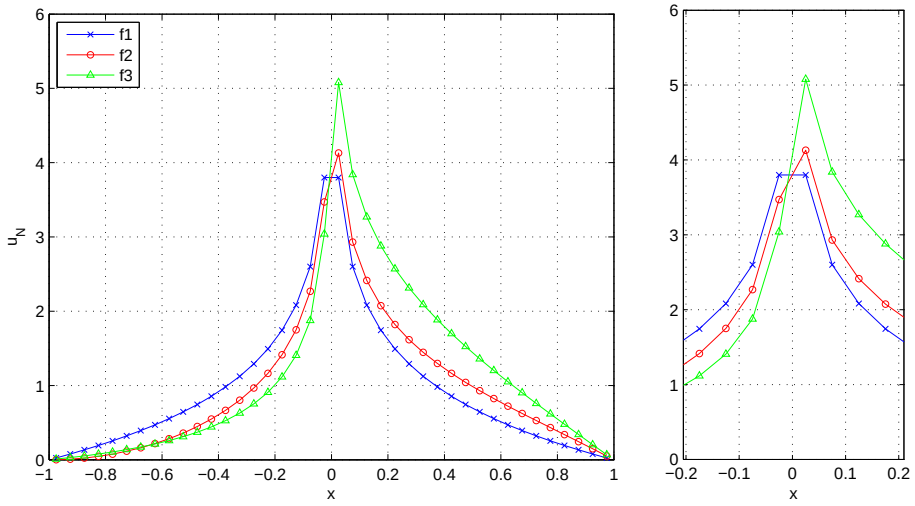

(a) (b)

FIGURE 8. **(a)** Numerical solutions u_N from nFVM with $b(x) = x$ and $f(x) = f_j(x)$ for the noncompatible case: $f_1(x) = 1$, $f_2(x) = x^3 + 1$, $f_3(x) = e^x$, $\epsilon = 10^{-4}$, $N = 40$; **(b)** Zooming near the transition layer.

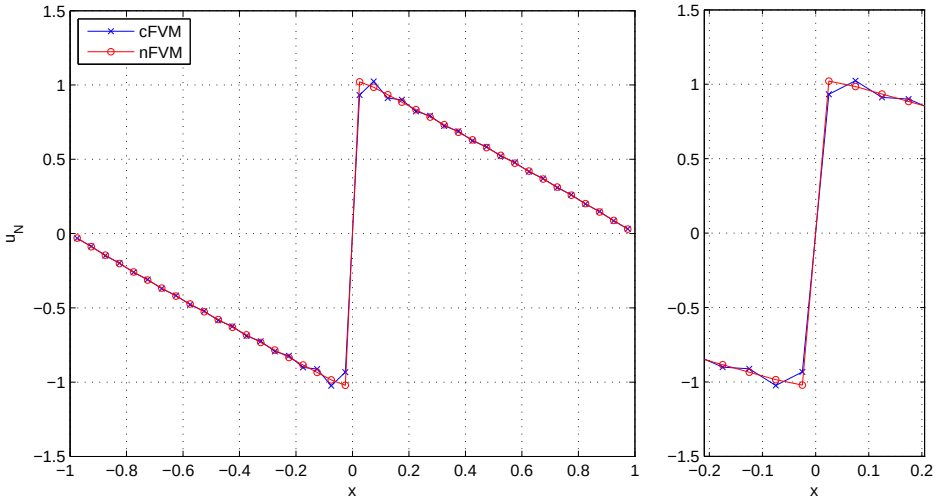

(a) (b)

FIGURE 9. **(a)** Numerical solutions u_N from cFVM vs. nFVM with $b(x) = \sin x$, $f(x) = x$, $\epsilon = 10^{-4}$, $N = 40$ for the compatible case; **(b)** Zooming near the transition layer.

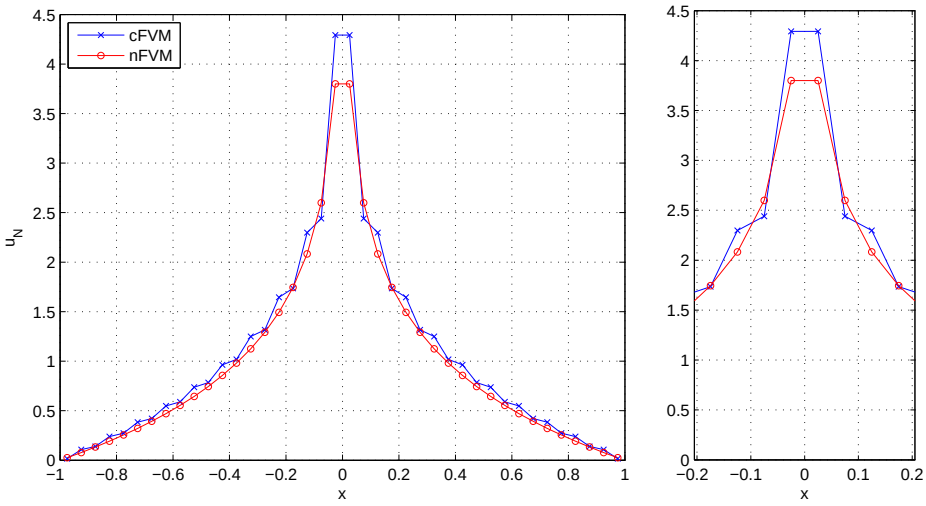

(a) (b)

FIGURE 10. **(a)** Numerical solutions u_N from cFVM vs. nFVM with $b(x) = \sin x$, $f(x) = 1$, $\epsilon = 10^{-4}$, $N = 40$ for the noncompatible case; **(b)** Zooming near the transition layer.